Alkali-surfactant foam improves extraction of oil from porous media

Zitha, Pacelli L.J.; Guo, Hua

DOI
10.1002/cjce.24379

Publication date
2022

Document Version
Final published version

Published in
Canadian Journal of Chemical Engineering

Received: 3 May 2021 | Revised: 19 August 2021 | Accepted: 12 October 2021

DOI: 10.1002/cjce.24379

SPECIAL ISSUE ARTICLE

THE CANADIAN JOURNAL OF CHEMICAL ENGINEERING

Alkali-surfactant foam improves extraction of oil from porous media

Pacelli L. J. Zitha | **Hua Guo**

Department of Geotechnology, Delft University of Technology, Delft, The Netherlands

Correspondence
Pacelli L. J. Zitha, Department of Geotechnology, Delft University of Technology, Stevingweg 1, 2628 CN Delft, The Netherlands.
Email: p.l.j.zitha@tudelft.nl

Abstract

Capillary forces result in the trapping of the oleic phase in porous media even after extensive flushing with brine. Alkali-surfactant-polymer formulations drastically diminish capillary forces, whereas adding polymer to the water phase increases viscous forces, resulting in highly efficient extraction of the residual oil. However, by virtue of its scale, the above process requires a large quantity of chemicals, which poses a threat to the environment. Here, we demonstrate that replacing the polymer with a gas such as nitrogen, flue gas, or carbon dioxide achieves equally superior oil extraction efficiency when using a much smaller amount of chemicals. Mobilized oil is first displaced as a continuous phase (oil-bank) and then as an oil-in-water dispersion. Microflow visualization experiments reveal that dispersed oil spreads at the gas–liquid interface (surfactant solutions) due to the presence of adsorbed surfactant molecules. Our dry-cleaning extraction of hydrocarbons has a wide spectrum of applications and is particularly useful for the production of hydrocarbons from underground formations while mitigating the impact of chemicals on the environment.

KEYWORDS

alkali, cleaning, dry, foam, oil, porous media, surfactant

1 | INTRODUCTION

Extraction of hydrocarbons or their derivatives from porous media plays a critical role in many industrial applications and scientific endeavours. Examples include extractive production of crude oil from deep geological formations,[1] clean-up of nonaqueous liquids phases from shallow subsurface,[2] and dry-cleaning of clothes stained by oily fluids.[3]

Production of crude oil, as a prototypical process, is done in three main stages. First, crude oil is expelled from the formation due to the expansion of hydrocarbons, water, and the compaction of formation rock. When pressure is too low to ensure further oil extraction, either water or gas is injected into the formation to increase the production. Extraction of hydrocarbons by these secondary recovery methods is limited due to two main mechanisms, operating at the microscopic and macroscopic levels. Microscopically, oil displacement by water or immiscible gas proceeds until the oleic phase disintegrates into blobs, which are immobilized at the largest pores due to capillary forces.[4] Capillary pressure

in porous media obeys the Young–Laplace equation $P_c = J(S_w)2\gamma\cos\theta/r$, where γ is the oil/water interfacial tension (IFT), θ is the oil/water/rock contact angle, r is the mean pore radius, and J (Sw) a monotonically decreasing function of water saturation (water volume fraction). Trapping of oil can be described in terms of the capillary number, defined as the ratio of viscous to capillary forces. On the other hand, macroscopically, contact between displacing water or gas and displaced oil may be severely limited due to viscous fingering, gravity segregation, and preferential flow through higher permeability streaks, also known as channelling.

Improving oil extraction beyond the above secondary recovery requires: (a) mobilization of residual oil and (b) improving sweep efficiency. Mobilization of residual oil is currently achieved either by drastically decreasing oil–water IFT controlling capillary forces[5] or, to a lesser extent, by treating porous media chemically to render it water- and oil repellent.[6] Carefully formulated alkali-surfactant systems reduce oil–water IFT by up to four orders of magnitude.[7] Sweep efficiency is improved by increasing aqueous phase viscosity, by adding hydrophilic polymers to it.[8] Such a conventional alkali-surfactant polymer (ASP) approach ultimately increases the volume fraction of the aqueous phase in the pores to nearly 100%. This implies that large quantities of chemicals are used, which could adversely impact the environment.[9]

The premise of the paper was that gas injection, instead of polymer, in conjunction with alkali-surfactant could yield superior oil extraction efficiencies, comparable to ASP, while using up to several times smaller amounts of chemicals. Such a dry extractive production method is particularly advantageous for low permeability media, for which polymer retention can cause severe clogging.[10] Successful extraction of oil by the above co-injection of gas and alkali-surfactant requires foaming of gas, that is, the dispersion of gas into liquid stabilized by a surfactant. In this innovative alkali-surfactant-foam (ASF) process, foaming imparts gas with a much higher viscosity than either water or oil, ensuring good sweep efficiency.[11–13] The ASF concept has been facing two main obstacles, namely,[14] (a) tendency of oil to destabilize foam and (b) difficulty in finding a single surfactant, which could provide ultralow oil–water IFT and be a good foaming agent.

This paper reports on a macroscopic porous media flow study showing that the two obstacles mentioned earlier can be lifted. The core-flood study reported by Guo et al.[15] is reinterpreted in combination with new microflow model studies to gain a better understanding of the ASF displacement processes.

2 | EXPERIMENTAL

2.1 | Materials and methods

Brine was prepared by dissolving pro-analysis sodium chloride (Fisher Scientific) in de-ionized water. Crude oil had an API gravity of 37.82 and a viscosity of 2.78 $\pm$ 0.01 cP at 60°C. The selected surfactant, an internal olefin sulphonate (IOS 2024, Stepan), was supplied in an aqueous solution with an active content of 73.0 $\pm$ 0.5 wt. %. Nitrogen gas supply from a 200 bar (1 bar = 100 kPa) cylinder was controlled using a pressure regulator and a mass-flow controller. Extensive preliminary screening of surfactants showed that IOS2024 had adequate foaming characteristics and the ability to generate ultralow IFT.[15]

The core-flood experiments were done using Bentheimer sandstone cylindrical core samples, with 3.8 $\pm$ 0.1 cm diameter and 17.0 $\pm$ 0.1 cm length. The porosity and permeability of the porous samples used were, respectively, 21 $\pm$ 1% and 1.2 $\pm$ 0.1 Darcy. The outcrop rock material was chosen because it is clean (it consists of more than 99% quartz), macroscopically homogenous, and isotropic.

2.2 | Setup and procedures

Gas and the formulated alkali-surfactant solution (AS) were co-injected into the sandstone cores using a high precision piston pump (Pharmacia P 500). Outlet pressure was kept at 2.0 MPa using an in-house made high precision backpressure regulator. Effluents were collected using a FRAC-200 fractional collector (Pharmacia Biotech). Gas and liquid injection rates, the pressure-drop, and liquid production rates were monitored using an in-house made data acquisition system. The core was CT scanned at time intervals during the experiments using a third-generation SAMATOM Volume Zoom Quad Slice CT scanner[16] to map the fluid saturations. The sequence of the macroscopic flow experiments was as follows: air was removed from the porous medium by flushing it with 99% CO_2 gas for 30 min at atmospheric pressure; about 10 PV of brine were injected at 0.5 ml/min, with backpressure first at 0.1 MPa till brine breakthrough and then at 2 MPa, to dissolve completely any remaining CO_2 and ensure 100% brine saturation; crude oil was injected downwards until irreducible water fraction $S_{wc} = 0.19 \pm 0.01$ was established (no more water production); brine was injected (5 PV) simulating water flooding process until irreducible oil fraction $S_{or} = 0.48 \pm 0.02$ was established; the porous medium was pre-flushed with 0.3 PV AS; finally, AS and N_2 were co-injected at 0.23/0.1 and 0.4 cm^3/min, respectively, to generate ASF (foam quality = 80%).

The visual flow cell embodies a quasi-two-dimensional (2D) flow pattern obtained by chemical etching of a glass plate. The etching process creates cylindrical pillars with diameters varying from 200–400 μm and having an average depth of nearly equal to 25 μm. The pillars are irregularly distributed over an area of 6 cm in the axial flow direction and 3 cm across, so that pore size ranged from 50–600 μm. The microflow model experiments were performed at room temperature and atmospheric pressure. The procedure for the micromodel experiment is similar to that used for the core-floods except for the absence of the AS pre-flush. The microflow model was first flushed with CO_2, evacuated, and then saturated with brine. Next, brine was displaced by crude oil until connate water saturation was reached, and then, the microflow model was waterflood until residual oil saturation was reached. Finally, N_2 gas and the AS solution were co-injected into the microflow model to generate the foam and mobilize the residual oil.

3 | RESULTS AND DISCUSSIONS

3.1 | Core-floods

The key finds from the core-flood experiments are depicted in Figure 1A–C. This figure was reported earlier by Guo et al.[15] but here we revisited and reinterpreted them afresh to form a coherent whole with the microflow model studies discussed in the next section. Figure 1A depicts oil saturation profiles along the length of the porous medium determined from the CT scan images after primary drainage (dark cyan), after imbibition (blue), and at two times during the AS pre-flush (red and black). A well-defined in-situ oil bank is formed during the AS slug injection. The spread of the transition zone behind the oil bank is due to the unstable displacement of the mobilized oil by the AS solution because the AS solution is less viscous than the oil. The transition from

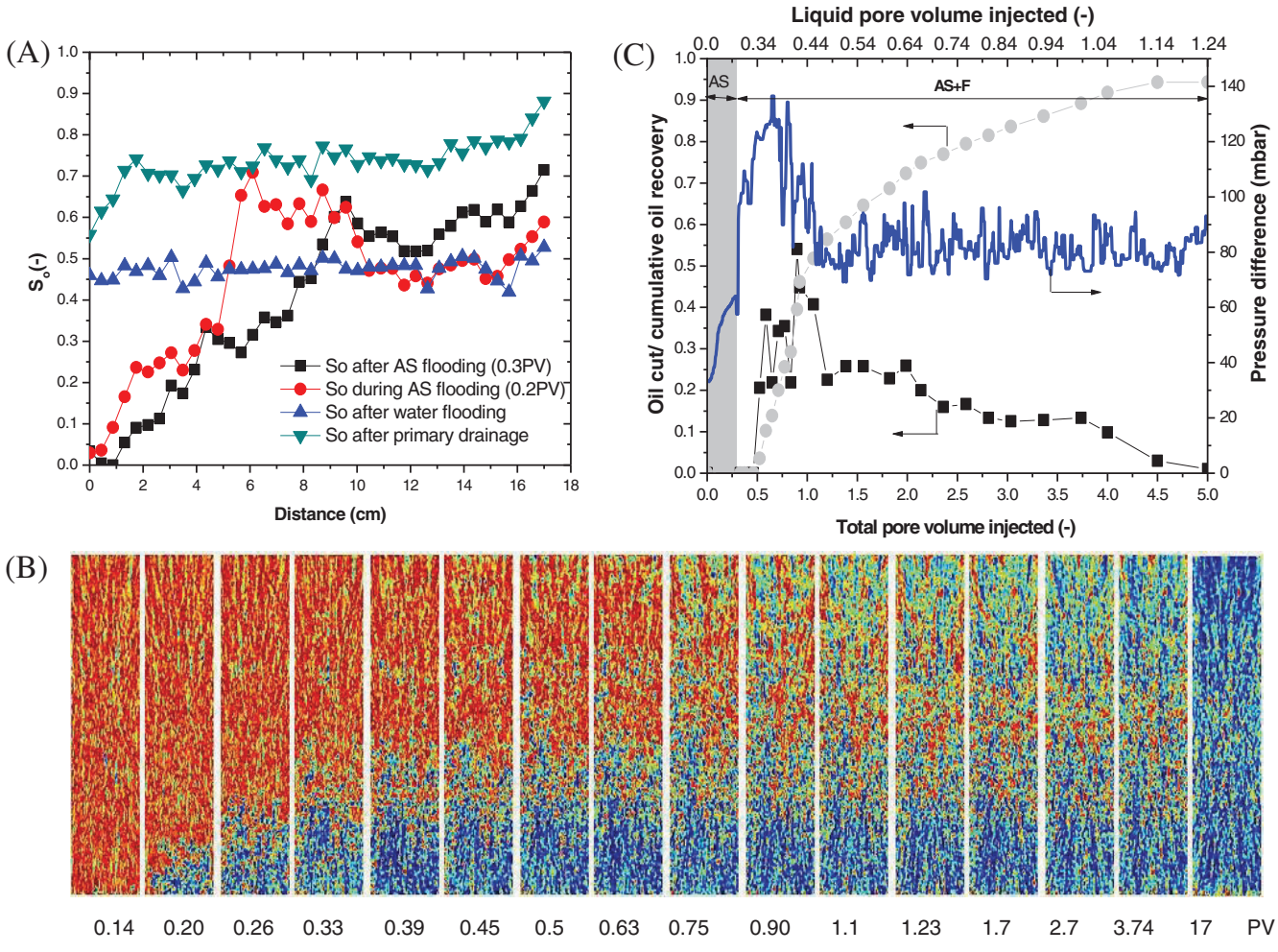

FIGURE 1 Characteristics of displacement in the alkali-surfactant-foam (ASF) process. (A) Oil saturation profiles determined from the CT images. (B) CT images of displacement profiles in the ASF drive process. (C) Efficiency of crude oil extraction by ASF from a Bentheimer sandstone sample and evolution of pressure drop (blue line). Cumulative recovery factor (grey circles). The oil bank breaks through at approximately 0.55 PV. A long tail-shaped production is observed after a sharp oil bank

the peak of oil in the bank ($S_o = 0.62$) to the remaining oil fraction after water-flooding ($S_o = 0.45$) is sharper for the opposite reason, although it is still slightly smoothed due to dispersion.

Figure 1B shows the CT scan images obtained for the ASF drive process, that is, during the co-injection of N_2 gas and AS following the AS pre-flush. PV = 0 corresponds to the start of the ASF drive. Stable foam generation is demonstrated by the frontal foam displacement, especially in the 0.33 PV, where the core has been well swept by the 0.3 PV AS pre-flush. The orange colour indicates the water-flooded residual oil, whereas the blue indicates gas and surfactant solution. The foam front seems stationary, but the fact that gas breaks through the outlet of the porous medium at 0.7 PV indicates that foam remains sufficiently stable even beyond 0.33 PV.

Figure 1C shows the oil cut in the effluents (black squares), the cumulative recovery factor (grey circles), and the pressure drop (blue line). The oil cut first rises steeply to a maximum value of 0.58, then drops sharply to 0.25, and finally diminishes slowly to nearly zero. Breakthrough of the oil bank occurs at approximately 0.55 PV and the long tailing oil production ensues, consistently with the saturation profiles and the CT scan images. The cumulative recovery factor increases first linearly to 0.48 and then at a diminishing rate to 0.95. The pressure drop, on the other hand, increases from 35 to about 65 mbar, first relatively steeply (between 0.08–0.15 PV) and then with a smaller slope. This behaviour corresponds essentially to the formation of the oil bank as the AS slug mobilizes the residual oil. The slower increase corresponds to the displacement of an already formed oil bank, which grows with further oil mobilization. During ASF flooding, pressure drop increases from 60–95 mbar as a result of the change in total injection rate from 0.23–0.5 cm^3/min upon switching from AS to AS and N_2 injection. The total flow rate was increased to allow accurate control of gas flow rate as the mass flow controller could not properly handle lower gas rates. After an initial jump, the pressure drop continued to rise, indicating good foam generation and propagation. The pressure drop reaches a maximum of about 125 mbar at 0.8 PV and then decreases. Finally, after 1.2 PV, the pressure drop stabilizes to an average plateau of about 85 mbar while showing fluctuations with an amplitude of about 20 mbar. The mobility reduction factor (MRF) corresponding to the plateau was estimated to be MRF = 1.22. An intriguing implication of these findings is that foam with a viscosity only slightly larger than that of brine provides sufficient mobility control to make ASF an enhanced oil recovery (EOR) process. To gain insight into these and other features, we examined residual oil recovery ASF from a visual microflow cell.

3.2 | Microflow analysis

Figure 2A shows a snapshot of the co-injection of N_2 and surfactant solution with a foam quality of 80% in the absence of oil. Note that the foam quality in this case was slightly lower than in the porous media case to prevent the foam from becoming too dry. Developed foam consists of bubbles of variable sizes separated from each other by lamella or larger bodies of fluids. As expected from earlier studies of foam in porous media, characteristic bubble and pore sizes were comparable.[17] Bubble coalescence or rupture was hardly observed during foam propagation; bubbles and lamellae proved to be highly deformable and crossed the smaller pores without splitting. This is probably due to the specific nature of the surfactant used, which gave the foam bubbles the unique ability to stretch and contract without breaking.[18-20]

To examine the influence of oil on the stability of foam, we co-injected AS and N_2 at the residual oil saturation condition. Figure 2B shows a snapshot of the foam texture in the presence of oil. It illustrates that foam bubbles formed near the injection point have propagated and spread over the entire cell surface. When bubbles contact oil, either oil spread on the bubble surface or formed a thin lens at the front of the bubble, that is, a pseudo-emulsion film, which travelled with bubbles. Spreading or lensing of oil at the N_2/AS interface had no noticeable effect on foam stability. It only caused the displacement of residual oil. This elucidates the observed tailing oil production regime in the macroscopic porous media. The absence of an oil bank in the visual microflow experiments can be explained by the fact that, since pores are very large, water injection was highly efficient in reducing the residual oil. Figure 2C illustrates the sequence of microscopic events observed when travelling foam bubbles came into contact with oil during flow from left to right. In the dashed circle, we traced one gas bubble to examine the formation and propagation of the lamella. The different phases were distinguished by the grey value of each phase in the image. At $t = 0$, the gas bubble had just been squeezed through the narrow pore throat when the front of the foam bubble came into contact with the oil blobs. At $t = 0.5$ s, the oil blob was emulsified into small droplets; the droplets were dislodged by the advance of the foam bubbles. In the meantime, the oil spreads on the front of the foam bubble. At $t = 1.0$ s, the foam bubbles continued to advance and made contact with the neighbouring gas bubbles. The pseudo-emulsion

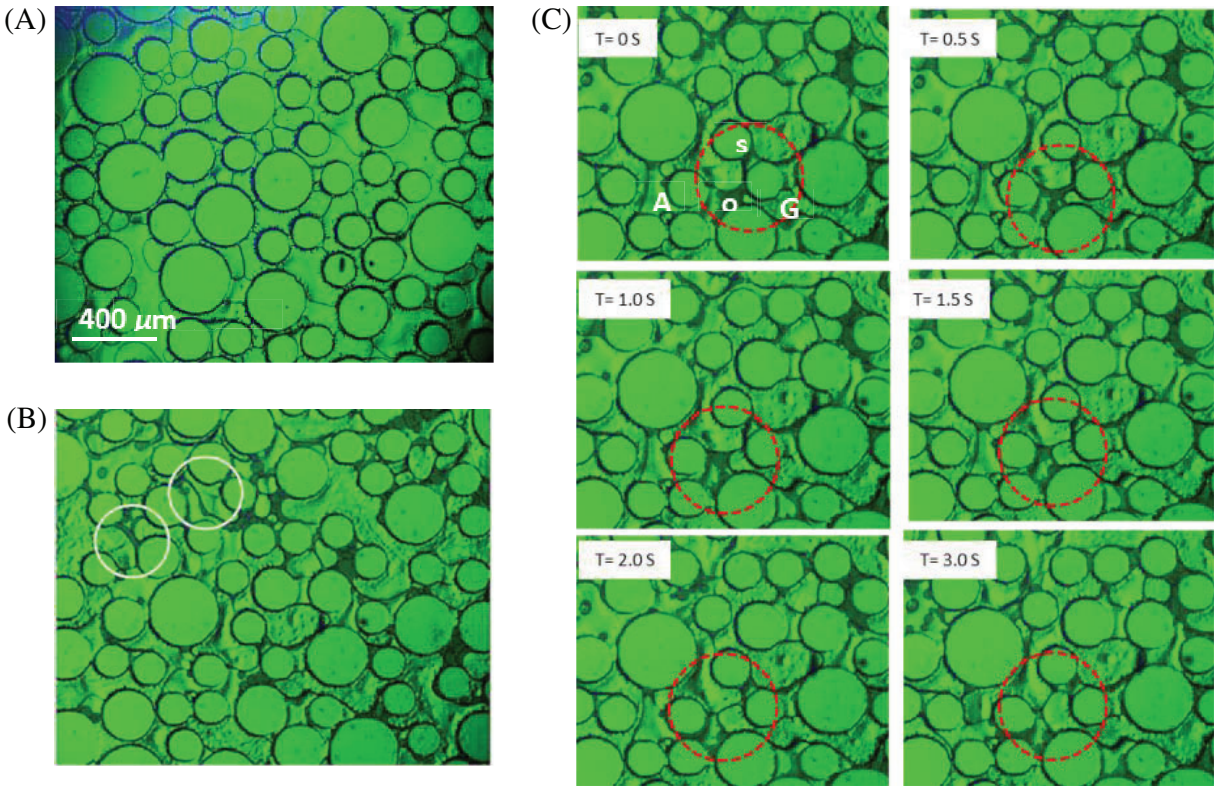

FIGURE 2 Direct visualization of foam propagation in the micromodel during the co-injection of alkali-surfactant solution (AS) and N_2 (flow is from left to right): (A) snapshot of the foam texture in the absence of oil. The foam flows from the inlet (right) to the outlet (left). Spherical objects are grains. (B) Snapshot of foam texture in the presence of the residual oil when foam propagates. (C) A sequence of microscopic events that occur when the travelling foam bubbles come into contact with the remaining oil. The solid, oil, aqueous, and gas phases are labelled S, O, A, and G, respectively

film was formed at the border of the gas/oil/aqueous phases. This film remained stable and moved forward regardless of the oil spreading on the surface. During the movement, the travelling liquid film started to elongate from 121–148 mm at $t = 1.5$ s and $t = 3.0$ s.

4 | CONCLUSIONS

We have demonstrated that ASF can efficiently extract oil from porous media when the amount of chemically activated fluids used is substantially reduced. The designed alkaline-surfactant formulation provided ultra-low IFT and proved to be a rather good foaming agent. The ASF achieved an extraction efficiency of nearly 100% in both macroscopic porous media and micromodel flow experiments. It was found that ASF extracts oil by a mechanism combining the formation of an oil bank and the transport of emulsified oil by flowing lamella. The visual flow experiments revealed that in the dispersed flow regime, oil extraction is due to oil spread at the gas–water interface.

ACKNOWLEDGEMENTS

This work was partially funded by grants from Shell Global Solutions. Our special thanks to the technical staff in the Dietz Laboratory at Delft University of Technology.

AUTHOR CONTRIBUTIONS

Pacelli L. J. Zitha: Conceptualization; data curation; formal analysis; funding acquisition; writing – review and editing. **Hua Guo:** Data curation; investigation; methodology; writing – original draft.

PEER REVIEW

The peer review history for this article is available at https://publons.com/publon/10.1002/cjce.24379.

DATA AVAILABILITY STATEMENT

The data that support the findings of article "Alkali-surfactant foam improves extraction of oil from porous media" by Pacelli Zitha (corresponding author) and Hua Guo are available from the corresponding author upon reasonable request.

REFERENCES

[1] G. C. Maitland, *J. Colloid Interf. Sci.* **2000**, *5*, 30.
[2] J. R. Hunt, N. Sitar, *Water Resour. Res.* **1988**, *24*, 1247.
[3] I. Johausson, P. Somasundaran, *Handbook for Cleaning/Decontamination of Surface*, 1st ed., Elsevier, Amsterdam, The Netherlands **2007**.
[4] S. Majid Hassanizadeh, W. G. Gray, *Water Resour. Res.* **1993**, *29*, 3389.
[5] R. L. Reed, R. N. Healy, in *Improved Oil Recovery by Surfactant and Polymer Flooding* (Eds: D. O. Shah, R. S. Schechter), Academic Press, Cambridge, MA **1997**, p. 383.
[6] S. Jafar Fathi, T. Austad, S. Strand, *Energ. Fuel.* **2011**, *25*(11), 5173.
[7] H. A. Nasr-El-Din, K. C. Taylor, *Colloid. Surface.* **1992**, *66*, 23.
[8] S. Liu, R. F. Li, C. A. Miller, G. J. Hirasaki, *SPE J.* **2010**, *15*(2), 282.
[9] R. D. Shupe, *J. Petrol. Technol.* **1981**, *33*, 1513.
[10] R. S. Seright, M. Seheult, T. Talashek, *SPE Reserv. Eval. Eng.* **2009**, *12*(5), 783.
[11] G. J. Hirasaki, J. B. Lawson, *Soc. Petrol. Eng. J.* **1985**, *25*, 176.
[12] A. R. Kovscek, C. J. Radke, *Fundamentals of Foam Transport in Porous Media in Foams: Fundamentals and Applications in the Petroleum Industry, ACS Advances in Chemistry Series*, Vol. N. 242, American Chemical Society, Washington, DC **1994**.
[13] R. F. Li, W. Yan, S. H. Liu, G. J. Hirasaki, C. A. Miller, *SPE J.* **2008**, *15*(4), 928.
[14] G. J. Hirasaki, C. A. Miller, M. Puerto, *SPE J.* **2011**, *16*(4), 889.
[15] H. Guo, R. Faber, M. Buijse, P. L. J. Zitha, *SPE J.* **2012**, *17*(4), 1186.
[16] P. L. J. Zitha, Q. P. Nguyen, P. K. Currie, M. A. Buijse, *Transport Porous Med.* **2006**, *64*(3), 301.
[17] G. A. Pope, B. Wang, K. Tsaur, *SPE J.* **1979**, *19*(06), 357.
[18] P. Nguyen, P. K. Currie, P. L. J. Zitha, *J. Colloid Interf. Sci.* **2004**, *271*(2), 473.
[19] S. Chen, Y. Zhou, G. H. Wang, W. J. Li, Y. Y. Zhu, J. N. Zhang, *J. Disper. Sci. Technol.* **2015**, *37*, 479.
[20] D. J. Manlowe, C. J. Radke, *SPE Reservoir Eng.* **1990**, *5*(4), 495.

How to cite this article: P. L. J. Zitha, H. Guo, *Can. J. Chem. Eng.* **2022**, 1. https://doi.org/10.1002/cjce.24379